Title	Molecular mechanisms of cell cryopreservation with polyampholytes studied by solid-state NMR
Author(s)	Matsumura, Kazuaki; Hayashi, Fumiaki; Nagashima, Toshio; Rajan, Robin; Hyon, Suong-Hyu
Citation	Communications Materials, 2: 15
Issue Date	2021-02-09
Type	Journal Article
Text version	publisher
URL	http://hdl.handle.net/10119/17052
Rights	(c) The Author(s) 2021. Kazuaki Matsumura, Fumiaki Hayashi, Toshio Nagashima, Robin Rajan and Suong-Hyu Hyon, Communications Materials, 2, 2021, Article number: 15. This article is licensed under a Creative Commons Attribution 4.0 International License, which permits use, sharing, adaptation, distribution and reproduction in any medium or format, as long as you give appropriate credit to the original author(s) and the source, provide a link to the Creative Commons license, and indicate if changes were made. The images or other third party material in this article are included in the article's Creative Commons license, unless indicated otherwise in a credit line to the material. If material is not included in the article's Creative Commons license and your intended use is not permitted by statutory regulation or exceeds the permitted use, you will need to obtain permission directly from the copyright holder. To view a copy of this license, visit http://creativecommons.org/licenses/by/4.0/.
Description	

COMMUNICATIONS MATERIALS

ARTICLE

https://doi.org/10.1038/s43246-021-00118-1 OPEN

Molecular mechanisms of cell cryopreservation with polyampholytes studied by solid-state NMR

Kazuaki Matsumura [1✉], Fumiaki Hayashi [2], Toshio Nagashima[2], Robin Rajan [1] & Suong-Hyu Hyon[3]

Polyampholytes are emerging macromolecular membrane non-penetrating cryoprotectants; however, the mechanism behind their cryopreservation remains unclear. Here, we investigated the mechanism using solid-state NMR spectroscopy. The polymer-chain dynamics and the water and ion mobilities in the presence of various membrane penetrating and non-penetrating cryoprotectants were monitored at low temperatures to mimic cryopreservation conditions. NMR experiments revealed that the water, Sodium-ion, and polymer-chain signals in a carboxylated poly-L-lysine (COOH-PLL) solution broadened upon cooling, indicating increasingly restricted mobility and increased solution viscosity. Moreover, strong intermolecular interactions facilitated the COOH-PLL glass transition, trapping water and salt in the gaps of the reversible matrix, preventing intracellular ice formation and osmotic shock during freezing; this reduced cell stress is responsible for cryoprotection. This simple NMR technique enabled the correlation of the cryoprotective properties of polymers that operate through mechanisms different from those of current cryoprotectants, and will facilitate the future molecular design of cryoprotectants.

[1] School of Materials Science, Japan Advanced Institute of Science and Technology, 1-1 Asahidai, Nomi, Ishikawa 923-1292, Japan. [2] Advanced NMR Application and Platform Team, NMR Research and Collaboration Group, NMR Science and Development Division, RIKEN SPring-8 Center, 1-7-22 Suehiro-Cho, Tsurumi-Ku, Yokohama City, Kanagawa 230-0045, Japan. [3] Joint Faculty of Veterinary Medicine, Kagoshima University, 1-21-24, Korimoto, Kagoshima 890-8580, Japan. ✉email: mkazuaki@jaist.ac.jp

Cryopreservation enables biological materials such as cells, tissues, and organs, to be preserved at ultra-low temperatures for desired periods of time, allowing them to be revived and restored as necessary. Although it is an under-investigated topic in the field of tissue engineering, cryopreservation has tremendous potential and is an indispensable tool in the biological, medical, and agricultural research fields, as well as in the clinical practice of reproductive medicine[1]. The first breakthrough in the field of cryopreservation was achieved by Polge et al. in 1949, when they reported that the addition of glycerol enables fowl sperm to be cryopreserved[2]. Dimethyl sulfoxide (DMSO) was subsequently found to efficiently cryopreserve red blood cells[3], which caught the attention of cryobiologists worldwide and became the most preferred cryoprotective agent (CPA), mainly because of its ability to penetrate cells. Although glycerol was eventually found to only exhibit weak cryoprotective properties, and DMSO is cytotoxic to cells[4–6], these CPAs were inevitably used because of a lack of efficient alternatives; hence, the development of more efficient CPAs is of paramount importance.

With the above discussion in mind, we previously developed a polyampholyte composed of carboxylated ε-poly-L-lysine (COOH-PLL) and found that it exhibited significant cryoprotective properties[7]. This membrane non-penetrating polymer agent affords excellent viability profiles for a number of cell types, including human mesenchymal stem cells and induced pluripotent stem cells[8–10]. Synthetic polyampholytes were also found to be extremely potent for cryopreserving cells[11–15]. However, the cryopreservation mechanism from the outside membrane remains unknown, which hinders the further expansion of polyampholytes as emerging macromolecular CPAs[16]. Gaining a clear understanding of how polyampholytes cryopreserve cells is not only of academic significance, but also increases the likelihood that polyampholytes will be successfully employed in regenerative medicines[17,18].

In this context, Gibson reported a synthetic polymer that exhibits cryoprotective properties for red blood cells because of its ability to suppress ice crystal growth[19–21], while Ben developed various polymeric and small-molecule CPAs that inhibit the recrystallization of ice[22,23]. In addition, it was recently reported that polymers with structures similar to DMSO exhibited high cryoprotective properties[24]. We previously observed that synthetic polyampholytes are highly cryoprotective because of their action in protecting cell membranes and suppressing ice recrystallization[11]; however, the molecular mechanism remains inconclusive, which limits the rational development of superior cryoprotective CPAs. Moreover, the effects of polymers on intracellular ice formation (IIF) has received little attention, despite IIF being the most important cause of cell damage and cell death during cryopreservation[25,26].

CPAs can be broadly classified into two categories based on their mode of action, namely penetrating and non-penetrating. Penetrating CPAs are small molecules, such as DMSO, glycerol, and ethylene glycol, and they preserve cells by reducing or avoiding ice formation during freezing, and by controlling the salt concentration[27]. As the formation of ice can exclude solute molecules during freezing, the electrolyte concentration in the remaining extracellular solution can increase, which is known as "freeze concentration,"[28–30] and this leads to cell dehydration to avoid IIF. A previous study with hydroxyethyl starch (HES), a non-penetrating CPA, suggested that it attracts and absorbs water from outside the membrane, thereby reducing the viscosity, increasing the rate of dehydration, and impeding intracellular ice crystal formation[31,32]. However, HES is weakly cryoprotective and is not suitable for all cell types. In contrast, polyampholytes are efficient CPAs that can be used for various cell types; hence, they should be better able to control dehydration from outside the membrane by controlling osmotic stress during freeze concentration.

In nature, intrinsically disordered proteins (IDPs), such as late embryogenesis abundant (LEA) proteins, protect organisms from dehydration stress caused by desiccation or osmotic stress at low temperatures[33–36]. Although IDPs have been speculated to protect desiccation-sensitive macromolecules by vitrification, the mechanism remains unclear. Since IDPs are charged molecules, like polyampholytes, they are good models for elucidating the mechanism behind desiccation tolerance. To the best of our knowledge, cryopreservation and desiccation have not been quantitatively analyzed from the viewpoint of dehydration control through the molecular structure.

Investigating polymer-chain dynamics is vital for elucidating the cryopreservation mechanism. It is known that a significant relationship exists between molecular motion and structure; molecular motion in a polymer arises through the interplay of thermal energy and cohesive forces between various fractions of the polymer chain, which is controlled by the polymer structure[37]. To date, a number of analytical techniques have been employed to ascertain the molecular motions of polymers; however they generally yield global molecular information. In contrast, nuclear magnetic resonance (NMR) spectroscopy provides site-specific and structural information; hence, qualitative and quantitative structural details can be extracted for frozen CPAs using solid-state NMR techniques[38].

Herein, we report our investigation into cell viability during freezing and thawing with CPA solutions, as well as the use of solid-state NMR spectroscopy to elucidate the mechanism behind the cryoprotective properties of polyampholytes. We also determine the soluble states and molecular mobilities of CPA, water, and salts at low temperatures to reveal the abilities of polyampholytes to control dehydration and suppress IIF during cryopreservation.

Results and discussion

Preparation and characterization of COOH-PLL. The controlled introduction of carboxyl groups into PLL was achieved by treatment with succinic anhydride (SA), which reacts with amino groups. As reported in our previous studies[7,9], the number of carboxyl groups introduced, as determined using the 2,4,6-trinitrobenzenesulfonate (TNBS) assay, was found to correspond with the feeding ratio and the obtained ^{1}H NMR results (Supplementary Table 1 and Supplementary Fig. 1). The carboxylation ratio shown in parentheses [e.g., PLL-(0.65)] indicates the fraction of α-amino groups that have been converted into carboxyl groups by treatment with SA (i.e., 65%). The osmotic pressure and pH were adjusted to 600 mOsm and 7.4, respectively, during the preparation of 7.5% polyethylene glycol (PEG), bovine serum albumin (BSA), and PLL-(0.65) solutions. When 10% DMSO was used, it was dissolved in saline solution without osmotic pressure or pH adjustments.

Cell viability after cryopreservation and IIF. The cell viabilities immediately after thawing the L929 cells cryopreserved with various polymer solutions and DMSO were examined, the results of which are presented in Fig. 1a, which shows that PLL-(0.65) and DMSO are significantly more cryoprotective than the other polymers. In a previous study, we showed that cell proliferation 6 h after thawing could be correlated with the cell viability immediately after thawing[7]. Therefore, the cryoprotective properties of each CPA can be compared by assessing the cell viability after thawing. Although ~10% DMSO is highly cryoprotective, it is inefficient at high concentrations owing to its high cytotoxicity.

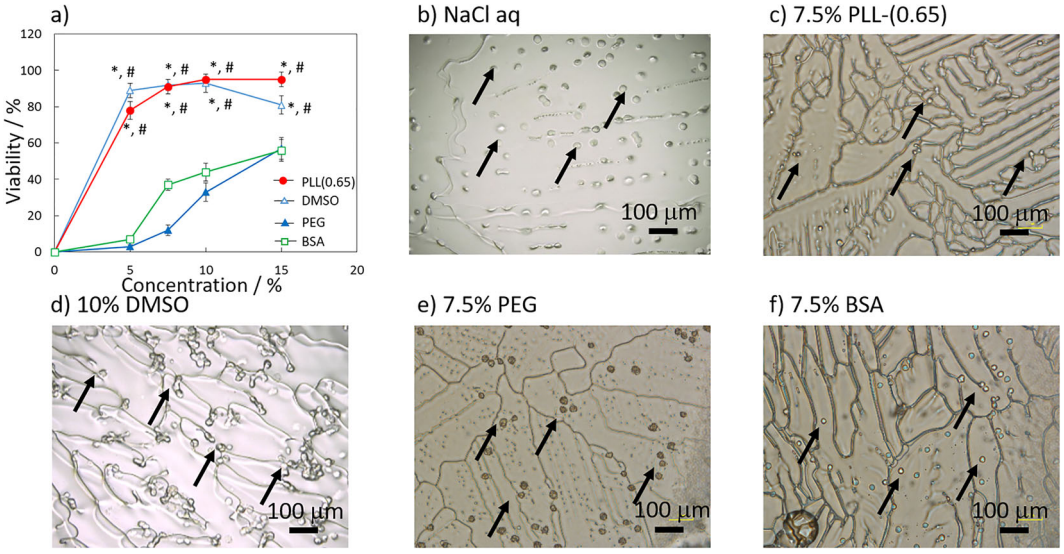

Fig. 1 Abilities of various CPAs to protect during cell freezing. a Cell viabilities after freezing with various CPAs. $^{*}p < 0.001$ vs. PEG, $^{\#}p < 0.001$ vs. BSA. **b–f** Cryomicroscopy images at −30 °C obtained by slow freezing (−1 °C/min) **b** without CPA and with **c** 7.5% PLL-(0.65), **d** 10% DMSO, **e** 7.5% PEG, and **f** 7.5% BSA. Arrows indicate representative cells during freezing. Scale bars: 100 μm.

The cell viability was found to depend on the polymer concentration following cryopreservation with BSA and PEG, although poorer results were obtained than with PLL-(0.65). Cells were not viable in the absence of the CPA (i.e., in saline solution alone). IIF during freezing is depicted in Fig. 1b–f, in which many cells are located in residual water sites in the DMSO and polymer solutions (Fig. 1c–f), and the cells shrink owing to freeze concentration. In contrast, almost no residual water was observed in saline solution (Fig. 1b), leading to considerable freeze concentration and cells located in ice components. It is well known that IIF is detectable by flashing under a cryomicroscope because ice crystals scatter light[39,40]. From a previous study, we know that IIF can occur during cooling or warming when the dehydration of cells during cooling is not sufficient to prevent free water inside the cells from undergoing crystallization[25]. As shown in the figure, the majority of cells in the PEG solution appear dark, which is indicative of crystallization and, consequently, IIF due to reduced cell dehydration. However, IIF was not observed in the saline, DMSO, PLL-(0.65), and BSA solutions indicating sufficient cell dehydration under these slow freezing conditions when ice seeding was employed at −2 °C to avoid supercooling. The ice seeding process involved the placing of a cooled needle on the surface of the cover glass at −2 °C to create ice nuclei, which then spread slowly. Without ice seeding, supercooling occurs and results in sudden crystallization. This causes cell damage; thus, ice seeding was adopted to avoid this. However, the viabilities of these cells differed significantly under these conditions; solid-state NMR spectroscopy was used to discuss this mechanism from the perspective of osmotic and dehydration stress relaxation by the CPA molecules (vide infra).

Behavior of water in ice using solid-state ^{1}H NMR spectroscopy: amount of residual water in ice. Solid-state NMR spectroscopy was used to investigate the mechanism and examine the polymer-chain dynamics. Residual water potentially protects cells during freezing since it provides additional space for cells to survive and prevents mechanical damage. The NMR spectra reveal the presence of diffusible molecules, which yield narrow signals, in contrast to the broad peaks observed for frozen components[41]. We, therefore, evaluated various CPA solutions under magic angle spinning (MAS) conditions to study the relationship between the amounts of residual water and solute, including the CPA. Representative water signals of the saline, 7.5% PLL-(0.65), 10% DMSO, 7.5% PEG, and 7.5% BSA solutions recorded between −1 and −41 °C are shown in Fig. 2a–e; only ice is present and no diffusible water is observed in the ^{1}H NMR spectrum of frozen pure water. However, as shown in Fig. 2, solutes can hydrate the water present in ice, resulting in solution-like behavior. In addition, the proton signal of water was observed to a decrease in intensity for each solution with decreasing temperature, with DMSO (Fig. 2c) giving the highest residual water ratio (>15%) over the entire temperature range, which implies that DMSO destroys the ordered structure of the water hydrogen bonding network to prevent ice formation. In contrast, the residual water content decreased in the presence of other CPAs (Fig. 2f). Interestingly, the residual water content for the PEG solution was significantly greater than that of the PLL-(0.65) solution at low temperatures. However, comparing their cryoprotective properties (Fig. 1) revealed contrasting behavior, with PLL-(0.65) exhibiting significant cryoprotective properties compared to BSA and PEG, which indicates that no direct relationship exists between the cryoprotective properties and the retention of residual water, and that the cryopreservation mechanism involving PLL-(0.65) differs from that of DMSO.

Behavior of water in ice using solid-state ^{1}H NMR spectroscopy: peak line width of the residual water present in ice. As the line width of a peak reflects molecular mobility, the line widths (full width at half maximum; FWHM) of the water protons in various solutions were measured at a range of temperatures (Fig. 2g). Water-molecule peak broadening in DMSO and in the saline solutions was slow, and the solution viscosities remained low at −41 °C. However, line broadening was rapid for the polymer solutions, with the PLL-(0.65) solution exhibiting significant broadening below −25 °C. Generally, the residual water present in a salt solution partially crystallizes and shows sudden discontinuous line broadening because of the phase transition. However, the water peak of the PLL-(0.65) solution exhibited severe line broadening, suggestive of an increase in the viscosity of non-crystallized water molecules, which can cause vitrification of the solution. Of relevance to this observation is the fact that the NMR peaks of water confined in mesoporous silica at

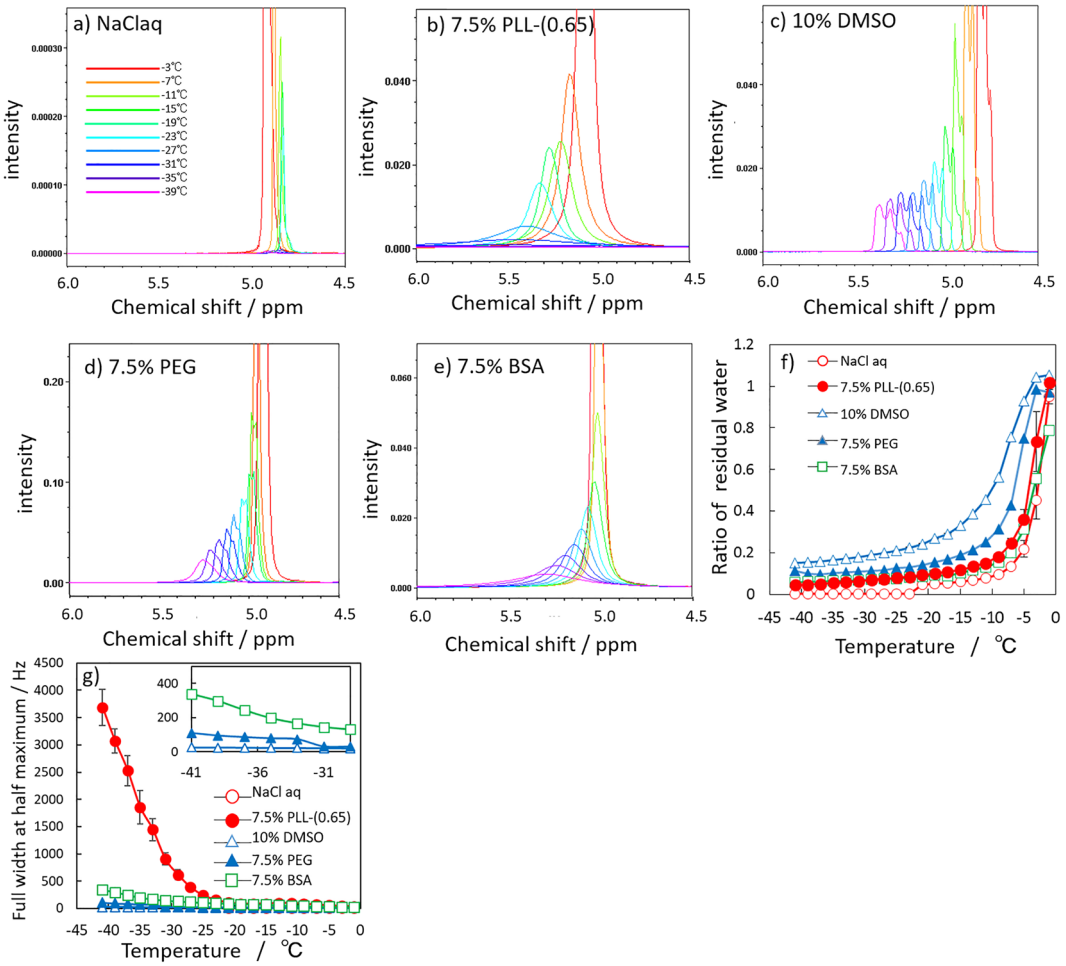

Fig. 2 Residual water determined by solid-state ^{1}H NMR spectroscopy. a–e ^{1}H signals of water at various temperatures in **a** saline solution, **b** 7.5% PLL-(0.65), **c** 10% DMSO, **d** 7.5% PEG. **e** 7.5% BSA. **f**, **g** Temperature-dependent **f** residual water ratio and **g** full-widths-at-half-maximum of the proton signals of various solutions. Inset in panel **g** represents an enlarged view. Error bars represent standard deviation.

low temperature were reported to show an additional broad component indicative of water vitrification or glass formation[42]. In addition, Fig. 2e, g shows an increase in the peak width at approximately −35 °C in BSA, whereas no such behavior was observed for the PEG solution above −41 °C (see Fig. 2g inset). It is therefore apparent that water mobility is most restricted in the PLL-(0.65) solution, followed by the BSA and PEG solutions, in which the viscosity of the water molecules increased. Compared with the results presented in Fig. 2f and g, it is apparent that comparable amounts of residual water exist in the PLL-(0.65) and BSA solutions; however, the mobility of the water molecules present in the residual water differed significantly, since the water molecules in PLL-(0.65) are highly restricted. Under such freeze concentration conditions, all solutes containing salts and polymers are highly concentrated, and as a result, the viscosity of the residual solution rapidly increased toward vitrification at approximately −25 °C, despite the glass-transition temperature of pure water being below −130 °C[43]. Investigating the temperature dependency of the spin–lattice relaxation time (T_1) enabled the simple determination of molecular mobility[44,45]. A local minimum in the T_1 relaxation time appears at the temperature where the molecular mobility is similar to the resonance frequency. The temperatures for the lowest water proton T_1 were −10 °C for PLL-(0.65) and −25 °C for PEG and BSA (Supplementary Fig. 2), which indicates comparable water-molecule mobilities under these conditions. The restriction of motion of salts and polymer chains and its effect on cryopreservation properties is discussed in subsequent sections.

Determining the salt ion state in ice using solid-state ^{23}Na NMR spectroscopy: line-width and line-shape analysis. The behavior of sodium ions in ice in the two-component (water-NaCl) system has been discussed previously[46], where Na ions in aqueous NaCl solution were found to remain diffusible even in the frozen state; however, all soluble parts transformed into eutectic crystals at the eutectic crystallization temperature (−21.2 °C). This was confirmed for our system using ^{23}Na NMR spectroscopy (Fig. 3). More specifically, the spectrum of the saline solution showed a narrow signal (indicative of a high diffusibility) at temperatures above the eutectic crystallization temperature, and complete peak disappearance below −21 °C (Fig. 3a). A similar line broadening behavior was observed to that of physiological saline above the eutectic temperature in the presence of other CPAs, such as DMSO (Fig. 3c); however, no phase transition was observed. The Na ions remained diffusible in DMSO even at lower temperatures. However, the Na signals broadened considerably with decreasing temperature for the PLL-(0.65), PEG, and BSA solutions (Fig. 3b, d, e). Line-shape analysis revealed that the Na peaks in the polymer solutions separate into two components during cooling, namely a sharp peak and a broad peak that were fitted by Lorentzian functions (Supplementary Figs. 3–5). These two peaks can be assigned to two types

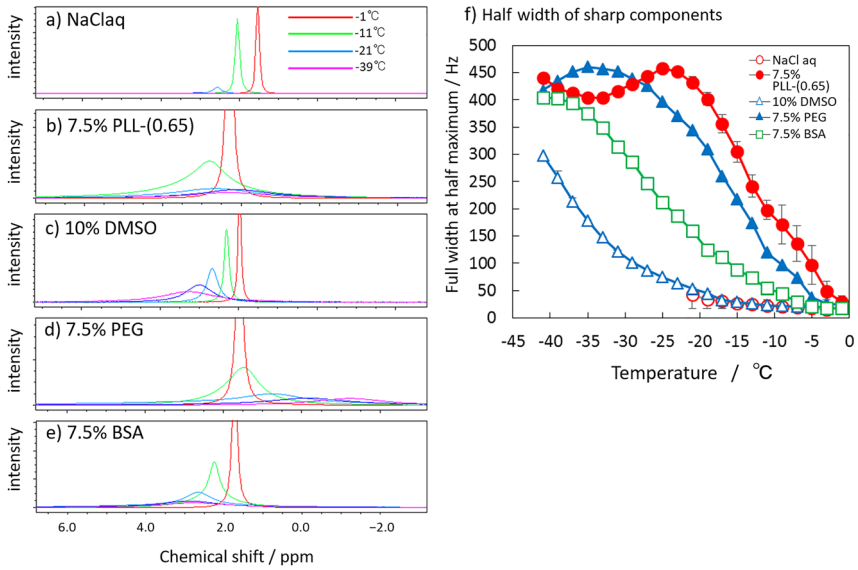

Fig. 3 Na-ion behavior of the CPAs at various temperatures. a–e Solid-state ^{23}Na NMR spectra of **a** the saline **b** 7.5% PLL-(0.65), **c** 10% DMSO, **d** 7.5% PEG, and **e** 7.5% BSA solutions. **f** Full-widths-at-half-maximum for the sharp components as functions of temperature. Error bars represent standard deviation.

Table 1 Relationship between the water and Na-ion behavior from the viewpoint of peak broadening.

	Temperature at which two components appear in the ^{23}Na NMR spectrum/°C (from Figs. 3f, 4c, and S3–S5)	Temperature at which severe broadening of the H_2O signal begins in the ^{1}H NMR spectrum/°C (from Figs. 2g and 4b)	Slope/Hz· °C^{-1} (average from −35 to −41 °C) (from Figs. 2g and 4b)
Physical meaning	Symmetry breaking in the electric field around the Na ions	Matrix begins to form	Rate of increase in viscosity for vitrification
Saline solution	No	No	No
7.5% PLL-(0.65) 600 mOsm	−7	−21	305.6
10% DMSO	No	No	0.65
7.5% PEG	−13	<−41	9.6
7.5% BSA	−5	<−37	23.5
7.5% PLL-(0.65) 1000 mOsm	−17	−29	205.4

of transition peaks for the Na ions. Since ^{23}Na is a quadrupolar nucleus, it yields a characteristic residual quadrupolar splitting, which is dependent on the asymmetry of the electric field. In a spatially uniform electric field, such as in the case of crystalline NaCl, only one signal can be obtained because all transitions are energetically equivalent. In addition, in an aqueous NaCl solution, owing to the uniform hydration around the Na ions, the obtained signal is a single peak. However, when the Na ion is located in an asymmetric electric field, the signals split into two components, namely a center transition and a satellite transition[47,48]. At low temperatures, the decrease in the number of mobile water molecules upon freezing results in penetration of the polymer chains into the second hydration shell of Na. This coordination of Na ions onto the polymer chains renders the electric field around the Na ions asymmetric, leading to the appearance of a satellite transition peak as a broad component. Compared with DMSO and the saline solution, the polymer solutions exhibited amplified broadening in the sharp components (Fig. 3f). This temporary broadening refers to the chemical exchange between the two states of Na ions, namely, the asymmetrical state resulting from coordination to the polymer chains and the symmetrical state. The physical meanings of the important parameters correlated between the behavior of water and the Na ions are outlined in Table 1 from the perspective of line broadening upon cooling.

We defined the temperatures at which twice the FWHM of the sharp components was smaller than the FWHM of the broad components as temperatures at which the broad components first appear (Table 1, column 2). This represents the disruption of symmetry (symmetry breaking) in the electric field around the Na ions. These temperatures were determined to be −5, −7, and −13 °C for the BSA, PLL-(0.65), and PEG solutions, respectively (Supplementary Figs. 3–5). At temperatures higher than these temperatures, the polymer-chain mobility is high, and so the duration of the coordination state is shortened and averaged by rotational diffusion motion, thereby resulting in the electric field appearing symmetrical on the NMR timescale. This indicates that the temperatures at which the chain mobilities of BSA and PLL-(0.65) are restricted are higher than that of PEG. The temperature at which the water proton signal begins to broaden significantly (Table 1 column 3) is the temperature at which the mobility of the water molecules begins to be suppressed, leading to the formation of a reversible polymer matrix, where the slope (Table 1, column 4) represents an increase in the viscosity of the solution toward solution vitrification. We define the matrix formation as reversible polymer aggregation because of the decrease in mobile water. The data presented in Table 1 indicate the symmetry breaking of the electric field around the Na ions in the PLL-(0.65) solution (i.e., coordination onto the polymer chains), which resulted in the asymmetry in the electric field around the Na

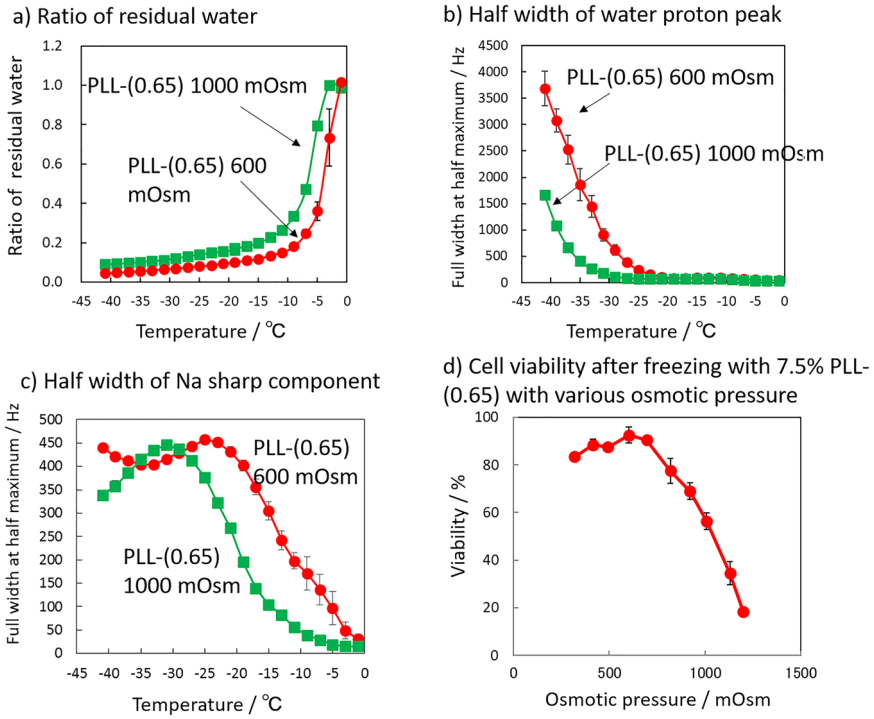

Fig. 4 Effect of a high salt concentration on the water, Na-ion behavior, and cryopreservation. a–c Temperature-dependent **a** ratio of residual water, full width at half maximum values for **b** the water proton peak, and **c** the Na sharp component signals of 600 and 1000 mOsm PLL-(0.65) solutions. **d** the cell viability after freezing with 7.5% PLL-(0.65) using various osmotic pressures. Error bars represent standard deviation.

ions emerging at −7 °C. In addition, at −21 °C, which is close to the eutectic crystallization temperature, the motion of the water molecules tends to become restricted; consequently, the viscosity begins to increase at a significantly higher temperature compared to the other polymer solutions, as indicated by the "slope" in Table 1. In contrast, the symmetry breaking of the electric field around the Na ions begins at −13 and −5 °C for the PEG and BSA solutions, respectively, even though motion of the water molecules was not restricted even at −41 or −37 °C, as indicated by only a slight increase in viscosity. Moreover, the increase in viscosity of the PEG and BSA solutions was also slower than that of the PLL-(0.65) solution, suggesting that the sodium ion and molecular water mobilities are restricted to greater extents in PLL-(0.65) than in PEG or BSA, which is likely owing to the presence of electrostatic interactions between the charged moieties in the polymer and the salts. These results indicate that vitrification of the PLL-(0.65) solution could begin at a higher temperature than for other polymer solutions.

Determining the salt ion state in ice using solid-state ^{23}Na NMR spectroscopy: effect of a high salt concentration on the water and Na-ion behaviors. A 7.5% PLL-(0.65) solution with a high salt concentration (i.e., 1000 mOsm) was also prepared to determine the effect of salt concentration. Figure 4a–c show the residual water content, the FWHM of the water signal, and the FWHM of the sharp Na component signal in a 1000 mOsm PLL-(0.65) solution. As indicated, the residual water content increased with increasing salt concentration (Fig. 4a), while the broadening temperature declined (Fig. 4b). In addition, the symmetry breaking in the electric field around the Na ion (−17 °C, Fig. 4c, Table 1, column 2), and restriction of the water-molecule mobility (−29 °C, Fig. 4b, Table 1, column 3) occurred at lower temperatures in the presence of higher salt concentrations. This suggests that the amount of residual water controls the viscosity of the polymer solution, resulting in lower vitrification temperatures in the presence of high salt concentrations. This result is consistent with the cryoprotective properties of PLL-(0.65), where a lower viability was observed for the 1000 mOsm solution (Fig. 4d). Comparing these results with the cell viability after cryopreservation using the various polymer solutions (Figs. 1 and 4d), the cryoprotective polymers must clearly simultaneously trap the salt ions and water molecules close to the eutectic crystallization temperature to evoke a rapid increase in the solution viscosity. Moreover, peak broadening (especially in the case of PLL-(0.65)) was also observed by ^{35}Cl NMR spectroscopy (Supplementary Fig. 6), which suggests that Cl ions are also trapped in the polymer chains undergoing solidification at low temperatures.

Determining the salt ion state in ice using solid-state ^{23}Na NMR spectroscopy: peak intensity and the Na concentration in ice. The relationship between the relative intensity of the ^{23}Na peak of each solution (i.e., the total amount of mobile Na ions) and temperature (Fig. 5a), reveals that eutectic crystallization occurs in the saline solution at approximately −21 °C, while no changes in intensity were observed for the DMSO and BSA solutions over the entire temperature region. In contrast, a considerable reduction in the Na-ion peak intensity was observed during freezing of the PLL-(0.65) solution, which is attributable to the decrease in the intensity of the sharp peak component. The PEG solution also exhibited a decrease in the Na peak intensity at low temperatures, but this was less evident than that in the case of PLL-(0.65). The temperature at which the decrease in the Na-ion intensity begins can be clearly correlated with the temperature at which the local maximum in the sharp component is observed (Fig. 3f). At such a temperature, the ratio of water molecules to Na ions is similar in all solutions (i.e., 10:1; Supplementary Table 2). The hydration number in the first hydration shell of Na ion has been reported to be approximately 4–6[49,50]. This indicates that polymer chains can begin to penetrate the first hydration

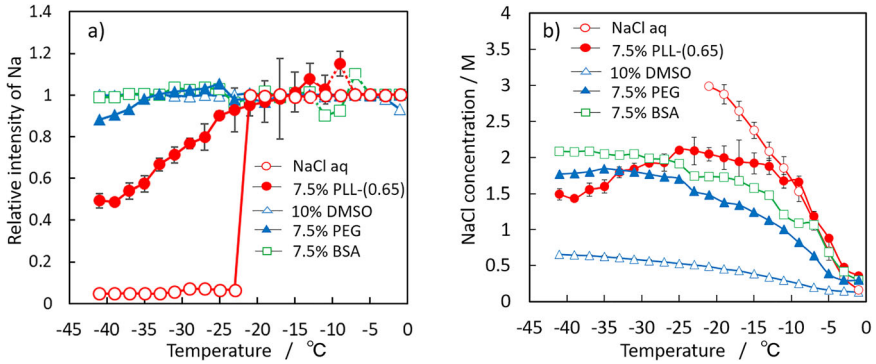

Fig. 5 Temperature dependent Na ion intensity and NaCl concentration in various CPA solutions. Temperature dependences of **a** Na-ion signal intensities and **b** NaCl concentrations calculated for various CPA solutions. The relative intensity values of the polymer solution in panel **a** above −15 °C are connected by dotted lines because it is difficult to separate the two components and there is a large degree of variation. Error bars represent standard deviation.

shell of Na ions because of the decrease in the amount of water molecules around the Na ions. It can be said that Na ions are trapped within the polymer chains, thereby the solidification of Na ions by restricting their mobilities at low temperatures could occur, especially in the case of PLL-(0.65), which exhibits higher electrostatic interactions than the other solutions.

Figure 5b shows the NaCl concentration for each solution as a function of temperature during freezing, as determined from the residual water and Na-ion ratios. We found that the NaCl concentration in the saline solution increased rapidly to ~3 M because of the low amount of unfrozen water resulting from freeze concentration. This rapid increase in salt concentration led to sudden cell dehydration because of a dramatic change in the osmotic pressure, resulting in severe dehydration damage, and accounting for the NaCl solution exhibiting no IIF in addition to a low cell viability (Fig. 1b). In addition, because of the phase transition by eutectic crystallization at −21 °C, sudden collapse by ice may result in physical damage to the cells. However, in the case of the DMSO solution, a less-dramatic initial increase in the salt concentration was observed because of the presence of larger amounts of residual water (Fig. 2f). Furthermore, DMSO can penetrate the cells to inhibit ice nucleation, thereby accounting for its IIF inhibition mechanism under less-dehydrating conditions[51], in addition to a high cell viability (Fig. 1d). In contrast, a distinct pattern was observed for the NaCl concentrations in the polymer solutions. More specifically, for the PEG solution, the NaCl concentration increased when cooled to −35 °C, beyond which a slight decrease was observed. The lower salt concentration in the PEG solution because of the presence of a higher residual water content therefore induces IIF and decreases the cell viability (Fig. 1e). However, in the case of PLL-(0.65), the NaCl concentration exhibited a more rapid increase than that observed in DMSO up to a temperature of −25 °C, after which the concentration began to decrease because of Na ion trapping. These results are consistent with the suppression of IIF (Fig. 1c) and the decrease in the Na-ion signal during freezing (Fig. 3). Similarly, in the case of BSA, the increased salt concentration dehydrates the cells sufficiently to suppress IIF (Fig. 1f); however, because of the lower charge density compared to that of PLL-(0.65), an excessive increase in salt concentration can result in higher dehydration damage in the case of BSA. From these results, it is possible that a critical salt concentration exists for inhibiting IIF, which is reached between the PEG solution and the PLL-(0.65) or BSA solution during freezing. These results clearly indicate that PLL-(0.65) efficiently protects cells from stresses, such as dramatic changes in osmotic pressure, in addition to controlling cell dehydration because of its ion-trapping properties at higher temperatures (Figs. 2g and 3f, Table 1).

Examining the behavior of the CPAs in ice using solid-state ^{1}H NMR spectroscopy: dynamics of the CPAs in ice. Investigating the mobility of a CPA in the frozen state can provide an understanding of the mechanism of water and salt trapping by a polymer matrix. With this in mind, we acquired the ^{1}H NMR spectra of various CPAs at different temperatures (Fig. 6). As expected, ^{1}H NMR experiments in the frozen state revealed contrasting behavior for the soluble states of the various CPAs. DMSO yielded particularly narrow signals (Fig. 6b), even when the temperature was lowered to −41 °C, suggesting that DMSO remains diffusible even at such low temperatures. PEG also exhibited a similar behavior, although peak broadening was observed below −31 °C, indicating a slight loss in mobility (Fig. 6c). In contrast, the BSA (Fig. 6d) and PLL-(0.65) (Fig. 6a) solutions showed signal broadening with only slight reductions in temperature. In the case of BSA, no peaks were detected below −15 °C, while PLL-(0.65) exhibited no peaks below −21 °C. These results unambiguously confirm that BSA and PLL-(0.65) lose their mobilities at these higher temperatures, and as a consequence, are unable to diffuse within the system. Based on the characteristic behaviors of water and the Na ions, in addition to the ^{1}H NMR results obtained at low temperatures for the polymer chains, it can be argued that the disappearance of these signals may be because of the glass transition of hydrated polymer chains caused by intermolecular interactions, especially in the case of PLL-(0.65). At temperatures below the glass-transition temperature, polymer chains lose their mobilities and form a reversible network matrix containing water and solute molecules. The solution vitrifies if the temperature is lowered sufficiently to restrict the motion of all molecules prior to crystallization[52]. In this context, reversible network matrix formation through electrostatic interactions between charged moieties may account for such aggregation through glass transition without precipitation. The severe broadening of the water proton signals shown in Table 1 is ascribable to the onset of reversible-matrix formation, during which the viscosity of the solution increases rapidly. It can be considered that through cooperative inhibition of the water-molecule mobility, the Na ions and polymer molecules form a matrix, which contributes to the vitrification of the solution at higher temperatures.

Overall, the ^{1}H NMR line broadening temperature decreased in the order: BSA > PLL-(0.65) > PEG » DMSO. However, BSA forms a higher-ordered three-dimensional (3D) structure, which restricts polymer-chain mobility. Polymer-chain movement within this 3D structure is limited by the formation of a secondary structure and hydrophobic side chain packing in the protein core, with the entire protein behaving like a rigid body such that even a slight increase in viscosity with decreasing

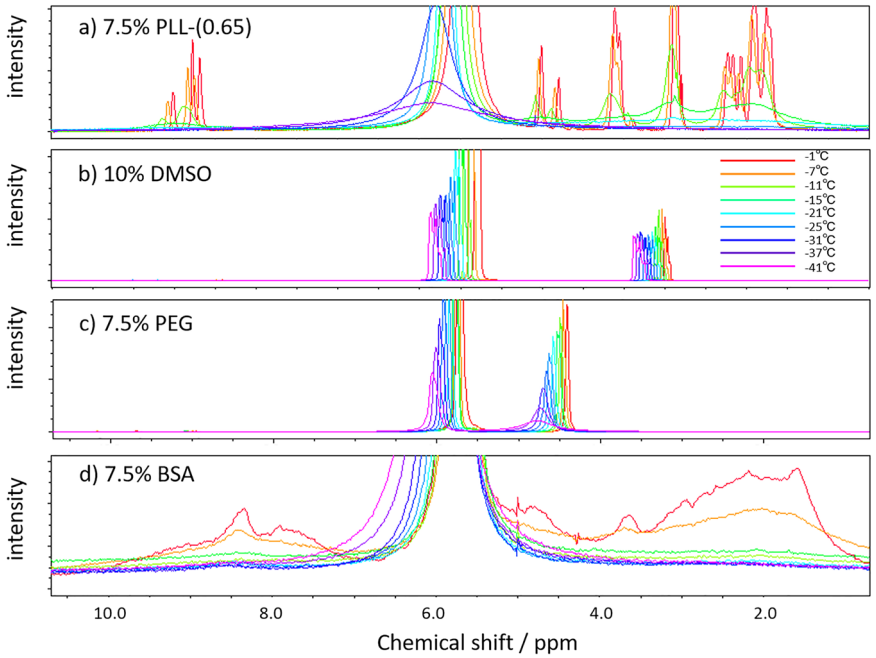

Fig. 6 Investigating the behavior of the ^{1}H NMR signals of various solutes over a range of temperatures. a–d Solid-state ^{1}H NMR spectra of **a** 7.5% PLL-(0.65), **b** 10% DMSO, **c** 7.5% PEG, and **d** 7.5% BSA.

temperature causes rapid broadening. In fact, no significant changes in the water and Na-ion signals were observed at −15 °C, indicating that rapid BSA-peak broadening is because of molecular contact with the globular protein. It indicates that the glass-transition temperature is lower than −15 °C, and is in good agreement with previous reports in which the glass-transition temperature of hydrated BSA was determined to be ~ −73 °C by dielectric measurements[53]. In contrast, PLL-(0.65) forms a reversible matrix between chains, as evidenced by cooperative changes in the water and Na-ion signals. Moreover, since PLL-(0.65) exhibits maximum line broadening for both Na^+ and Cl^-, it appears that this reversible matrix also traps Na^+ and Cl^- to avoid dramatic changes in the osmotic pressure.

In previous studies, cells undergo IIF not only because of spontaneous crystallization within the cells, but also because of seeding by extracellular ice crystals through aqueous channels in the cell membrane. According to a study by Mazur, IIF observed at a temperature above −40 °C, which is normally found in the range of −5 to −15 °C, could be attributed to extracellular ice[25]. In addition, Toner modified the model of IIF that is catalyzed by the plasma membrane or by internal particles after extracellular ice formation at the corresponding temperature ranges of −5 to −20 °C, and −30 to −35 °C, respectively[54]. An increase in viscosity of the polymer solution prevents the diffusion of ice nucleation, leading to the inhibition of seeding by extracellular ice. At a temperature above −40 °C, the large increase in the viscosity of PLL-(0.65) could inhibit the IIF caused by extracellular ice.

Examining the behavior of the CPAs in ice using solid-state ^{1}H NMR spectroscopy: polymer-chain dynamics of PLL-(0.65) at various osmotic pressures. The polymer-chain dynamics of PLL-(0.65) were then examined at various osmotic pressures, as presented in Supplementary Fig. 7. Interestingly, the polymer chains retained a significant mobility as the salt concentration was increased to 1000 mOsm, which was because of the increase in residual water at lower temperatures (Fig. 4a). This behavior correlates well with the observed cryopreservation properties of PLL-(0.65) at different osmotic pressures (Fig. 4d), where a higher osmotic pressure leads to a lower post-thaw cell viability. If the salt concentration is low, the viscosity of the polymer tends to increase, however, dehydration becomes insufficient. If the salt concentration is high, the viscosity does not increase sufficiently at low temperatures, despite the fact that the dehydration effect on cells is high. Taken together with the results presented in Table 1, it is apparent that the Na ion trapping and matrix-formation temperatures decrease at higher osmotic pressures due to an increase in the amount of residual water, strongly suggesting that interactions between the polymer chains are weakened in the presence of salts, which lowers the temperature at which the viscosity increases. This result clearly indicates that increasing the viscosity of the solution toward vitrification at higher temperatures through freeze-concentration-induced reversible-matrix formation is critical for the cryopreservation of cells because of the action of IIF inhibiting stimulated by an inflow of extracellular ice crystals.

To further elaborate this point, we studied the ^{1}H NMR spectra of COOH-PLL at various COOH substitution ratios. In the absence of COOH substitution (i.e., a positively charged polymer), the polymer chains retained a considerable mobility (low viscosity) at lower temperatures, while increasing the carboxylation ratio (i.e., neutralizing the polymer) tended to reduce the chain mobility (higher viscosity) at lower temperatures (Supplementary Fig. 8a–d). In addition, a higher COOH substitution resulted in an improved viability (Supplementary Fig. 9), which correlates with an increase in viscosity. In other words, the polymer-chain mobility began to decrease with further increases in the degree of COOH substitution, with the highest loss of mobility being observed for PLL-(0.65). However, the differences between the samples are not large, and the cation toxicity may also affect the cell viability in less-carboxylated PLL solutions. Thus, the presence of oppositely charged ions in the polymer chain (i.e., a polyampholyte structure) is necessary to achieve good cryoprotective properties.

The increase in the COOH-PLL viscosity as the temperature was lowered can be ascribed to the onset of the glass transition, where a relatively high glass-transition temperature is caused by

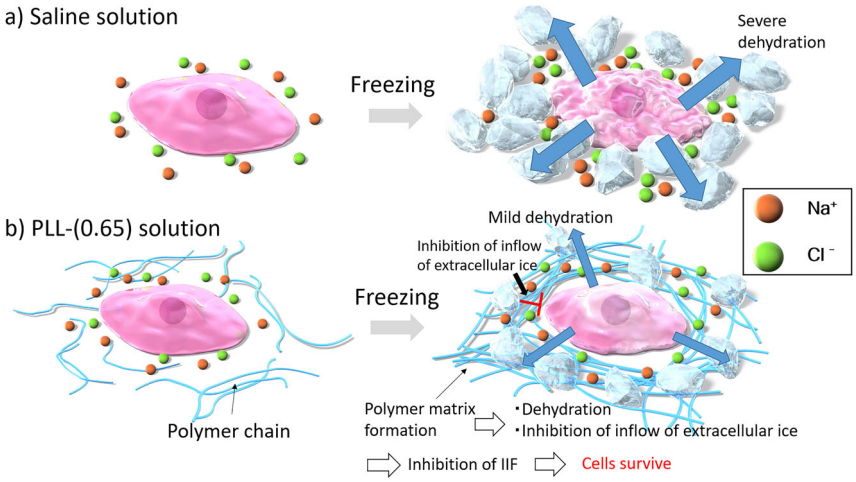

Fig. 7 Schematic illustration of the mechanism of cryoprotection by PLL-(0.65). a When the cells are frozen in saline solution, excessive cell dehydration occurs because of the severe freezing concentration, leading to lethal dehydration damage. **b** When the cells are frozen with PLL-(0.65), the polymer molecules aggregate because of strong intermolecular electrostatic interactions caused by freeze concentration, thereby trapping ions and water in the matrix to reduce any dramatic osmotic change. The viscous polymer matrix inhibits the inflow of extracellular ice to avoid IIF.

the presence of appropriate intermolecular interactions between the negatively and positively charged groups present in COOH-PLL. This is in agreement with the previously established understanding of the glass transition of a polymer, which is greatly influenced by intermolecular interactions, such as hydrogen bonding, van der Waals interactions, dipole-dipole forces, and induction forces[55–57]. By measuring the water, salt, and polymer-chain dynamics using solid-state NMR, we proposed a reasonable mechanism behind the cryoprotection properties of the PLL-(0.65) solution.

More specifically, we studied the cryoprotective properties of COOH-PLL, a membrane non-penetrating polyampholyte. Interestingly, the cells cryopreserved with this polymer exhibited excellent post-thaw viabilities. Comprehensive mechanistic investigations were therefore carried out using solid-state NMR spectroscopy during freezing. The results reveal that a polyampholyte can cryopreserve cells by forming a matrix around the cell membrane during freezing, which also traps salts to prevent osmotic damage, while ensuring sufficient dehydration to prevent spontaneous IIF (Fig. 7). In addition, the rapid increases in viscosity at higher temperatures are important for the facile attainment of solution vitrification to inhibit the IIF caused by the inflow of extracellular ice. Retention of the highly viscous solution status at higher temperatures due to matrix formation was also observed, which prevents recrystallization during thawing in addition to sufficient dehydration. These results agreed well with previous research, which reported that the glassy state could be stabilized by the polyampholytes[58–60].

These findings can also be used to explain the mode of action of protection against similar stress-induced damage. For example, LEA proteins are known to fold into amphipathic class A α-helix conformations upon desiccation and also in the presence of NaCl[61,62]. These helices contain both positive (on two opposing sides at the polar-nonpolar interface) and negative (at the center of the polar face) charges[61] and, as such, they behave as polyampholytes. The desiccation tolerances of these proteins have been attributed to their abilities to protect the mitochondrial membrane from osmotic stress[36], their roles as molecular shields[35], their abilities to kinetically stabilize aggregating proteins[63], and their preferential adsorption at air-water interfaces[34] through sugar-assisted vitrification[64,65]. Owing to the polyampholytic nature of LEA proteins, the results obtained with our polyampholytes can be extrapolated to LEA proteins. It can therefore be argued that LEA proteins trap ions during desiccation, which in turn reduces osmotic damage to the membrane. In addition, in the case of tardigrades, IDP not only assists desiccation tolerance, but also prevents freeze damage, and it is well-established that both drying and freezing processes induce osmotic damage[33]. The development of a complete understanding of the mechanism of polymeric CPA and LEA proteins is expected to enable the design of smart materials for these applications in the future.

Conclusion. In conclusion, we herein investigated the mechanism of cell cryopreservation by polyampholyte membrane non-penetrating CPA using solid-state NMR spectroscopy. The mechanism of cryoprotection imparted by carboxylated poly-L-lysines (COOH-PLLs) revealed by this technique can be summarized as follows:

(1) Cell dehydration from the outside under mild conditions suppresses IIF. This is achieved by controlling osmotic pressure through the trapping of salts and water molecules in the polymer matrix. (2) Maintaining a viscous state at higher temperatures inhibits IIF caused by the inflow of extracellular ice.

Through the use of this simple NMR technique to monitor peak line broadening upon cooling, we evaluated the cryoprotective properties of polymers based on the ease by which glass transition is attained. Through molecular design to satisfy the above conditions and taking into consideration the bulkiness of the side-chains, the main-chain mobility, the molecular weight, and the charge density, in addition to the design of superior CPAs, we expect that it will be possible to develop even highly effective non-polyampholyte CPAs. This study also opens up potential new avenues for understanding the similarities between naturally derived desiccation-tolerant proteins and synthetic functional materials from the viewpoint of the polyampholyte structure. Moreover, a comprehensive understanding of the cryopreservation mechanism is expected to promote the clinical use of such polymeric CPAs and advance the molecular design of much-needed novel polymeric CPAs that can serve as efficient alternatives to small-molecule CPAs such as DMSO and glycerol. Studies into the COOH-PLL–mediated cryopreservation of 3D tissue constructs for clinical applications in regenerative medicine are currently ongoing in our group, and the results will be presented in due course.

Methods

Materials. The 25% (w/w) aqueous ε-poly-L-lysine (PLL, MW 4000) solution was purchased from JNC Corp. (Tokyo, Japan). PEG (MW 3000), BSA, SA, and 2,4,6-trinitrobenzenesulfonate (TNBS) were purchased from Wako Pure Chemical Ind. Ltd. (Osaka, Japan). All materials were of reagent grade and were used without further purification.

COOH-PLL preparation. COOH-PLL was prepared as described in our previous study[7]. More specifically, a 25% (w/w) aqueous PLL aqueous solution was mixed with SA at molar ratios ranging from 0 to 100% (SA/PLL amino groups) and incubated at 50 °C for 1 h to convert the amino groups into carboxyl groups. The number of amino groups was determined using the TNBS method[66]. In this step, the sample solution (0.3 mL, 250 mg/mL), the TNBS solution (1 mL, 1.0 mg/mL), and an aqueous sodium bicarbonate solution (2 mL, 40 mg/mL) containing 10 mg/mL sodium dodecyl sulfate (pH 9.0) were mixed and incubated at 37 °C for 2 h. After this time, the mixture was cooled to 25 °C, and the absorbance was measured at 335 nm. The ratio of carboxylation, which was determined by the TNBS assay and ^{1}H NMR spectroscopy and indicated in parentheses [e.g., PLL-(0.65)], suggested that 65% of the α-amino groups had been converted into carboxyl groups by SA addition.

Cell culture. L929 (mice fibroblast cell line, American Type Culture Collection, Manassas, VA, USA) cells were cultured in Dulbecco's modified Eagle's medium (DMEM, Sigma Aldrich, St. Louis, MO) supplemented with 10% fetal bovine serum (FBS). Cell culturing was carried out at 37 °C under 5% CO_2 in a humidified atmosphere. When the cells reached 80% confluence, they were removed using 0.25% (w/v) trypsin containing 0.02% (w/v) EDTA in PBS (−) and seeded on a new tissue culture plate for subculturing.

Cryopreservation protocol. The cryopreservation solutions were prepared as follows: COOH-PLL was dissolved in DMEM without FBS at a concentration of 7.5% (w/w), and the pH was adjusted to 7.4 using 5 M HCl or NaOH. The osmotic pressure was measured using an osmometer (Osmometer 5520; Wescor, Inc. UT, USA) and was adjusted to ~600 mOsm for cryopreservation solutions of PLL derivatives using a solution of 10% NaCl. The cells were counted and re-suspended in 1 mL volumes of saline solutions of COOH-PLL, PEG, BSA, and DMSO with various concentrations at a density of 1×10^6 cells/mL in 1.9 mL cryovials (Nalgene, Rochester, NY) and stored in a −80 °C freezer after cooling at a rate of −1 °C/min in a controlled freezing container (Mr. Frosty, Nalgene) over 1 w.

Cell viability assay. Individual vials were thawed in a water bath at 37 °C with gentle shaking, after which the thawed cells were diluted in DMEM. Following centrifugation, the supernatant was removed, and the cells were re-suspended in DMEM (5 mL). To determine the cell survival, the medium was collected, and all cells were stained with trypan blue and counted using a hemocytometer immediately after thawing. The reported values are the ratios of living cells to the total number of cells.

Cryomicroscopy. The L929 cells were observed during freezing in saline solution or in the cryopreservation solution (10% DMSO, 7.5% PLL-(0.65), 7.5% PEG, and 7.5% BSA) using a cryomicroscope. An aliquot (4 μL) of the cell suspension was pipetted in the center of a quartz crucible (15 mm in diameter), covered, loaded on a cooling stage (Linkam 10002L Cooling Stage, Linkam Scientific Instruments, UK), and cooled to −30 °C at a rate of 1 °C/min. Ice was seeded at −2 °C using a needle that had been precooled in liquid nitrogen to avoid supercooling. Cell morphology was captured using a mounted photomicroscope at −30 °C (Digital Microscope, VHX-500, Keyence Corp., Tokyo, Japan).

NMR measurements. Solid-state NMR experiments were performed on a 700-MHz JEOL ECA spectrometer (JEOL, Tokyo, Japan), using a Doty Scientific Inc. (DSI) 4 mm HXY CP/MAS NMR probe. In these experiments, a 10% DMSO saline solution was used as the CPA control, a 7.5% PLL-(0.65) saline solution was used as the sample solution, 7.5% BSA and 7.5% PEG saline solutions were employed as weakly charged polyampholyte and the non-ionic polymer solution control, respectively, and a 0.9% aqueous solution of NaCl (physiological saline solution) was also used. The solution samples containing a CPA agent were sealed in DSI inner-sealing cells for an XC4 rotor and were spun at 3.6–5.8 kHz at temperatures ranging from 1 to −41 °C. The sample was cooled by replacing the spinning and bearing gases with cooled N_2 gas obtained by passing through a liquid nitrogen cryostat using a DSI cold gas supply unit. All ^{1}H, ^{23}Na, and ^{35}Cl data were collected over a single pulse experiment, providing sharp signals from the soluble part. All data were processed using NMRPipe[67] or Delta ver. 5.1.3 (JEOL). NMRView][68] or Delta ver. 5.1.3 (JEOL) was employed for spectral visualization and analysis. The peak intensities and line widths were analyzed by IGOR (WaveMetrics) or Delta ver. 5.1.3 (JEOL). The contribution from the frozen components or baseline roll was eliminated by baseline correction and line-shape analyses. The amount of residual water and soluble salt in the ice were estimated by the peak intensities of the H_2O, Na^+, and Cl^- ion signals. The volume of CPA was taken into account when calculating the salt concentration of the liquid present within the ice, assuming that the specific gravity of COOH-PLL is 1 g/cm^3.

Statistical analysis. All data are expressed as the means ± standard deviations. The Tukey–Kramer test was used to compare data among more than three groups. Differences with p values <0.05 were considered statistically significant.

Reporting summary. Further information on research design is available in the Nature Research Reporting Summary linked to this article.

Data availability

The experimental data that support the findings of this study are available from the corresponding author upon reasonable request.

Received: 10 November 2019; Accepted: 5 January 2021;
Published online: 09 February 2021

References

1. Rajan, R. & Matsumura, K. *Development and Application of Cryoprotectants. in Survival Strategies in Extreme Cold and Desiccation: Adaptation Mechanisms and Their Applications* (eds Iwaya-Inoue, M., Sakurai, M. & Uemura, M.) 339–354 (Springer Singapore, 2018).
2. Polge, C., Smith, A. U. & Parkes, A. S. Revival of spermatozoa after vitrification and dehydration at low temperatures. *Nature* **164**, 666 (1949).
3. Lovelock, J. E. & Bishop, M. W. H. Prevention of freezing damage to living cells by dimethyl sulphoxide. *Nature* **183**, 1394–1395 (1959).
4. Fahy, G. M. The relevance of cryoprotectant "toxicity" to cryobiology. *Cryobiology* **23**, 1–13 (1986).
5. Oh, J.-E. et al. Cytoskeleton changes following differentiation of N1E-115 neuroblastoma cell line. *Amino Acids* **31**, 289–298 (2006).
6. Young, D. A. et al. Expression of metalloproteinases and inhibitors in the differentiation of P19CL6 cells into cardiac myocytes. *Biochem. Biophys. Res. Commun.* **322**, 759–765 (2004).
7. Matsumura, K. & Hyon, S.-H. Polyampholytes as low toxic efficient cryoprotective agents with antifreeze protein properties. *Biomaterials* **30**, 4842–4849 (2009).
8. Matsumura, K., Bae, J. Y. & Hyon, S. H. Polyampholytes as cryoprotective agents for mammalian cell cryopreservation. *Cell Transplant.* **19**, 691–699 (2010).
9. Matsumura, K., Hayashi, F., Nagashima, T. & Hyon, S. H. Long-term cryopreservation of human mesenchymal stem cells using carboxylated poly-l-lysine without the addition of proteins or dimethyl sulfoxide. *J. Biomater. Sci. Polym. Ed.* **24**, 1484–1497 (2013).
10. Matsumura, K., Bae, J. Y., Kim, H. H. & Hyon, S. H. Effective vitrification of human induced pluripotent stem cells using carboxylated epsilon-poly-l-lysine. *Cryobiology* **63**, 76–83 (2011).
11. Rajan, R., Hayashi, F., Nagashima, T. & Matsumura, K. Toward a molecular understanding of the mechanism of cryopreservation by polyampholytes: cell membrane interactions and hydrophobicity. *Biomacromolecules* **17**, 1882–1893 (2016).
12. Rajan, R., Jain, M. & Matsumura, K. Cryoprotective properties of completely synthetic polyampholytes via reversible addition-fragmentation chain transfer (RAFT) polymerization and the effects of hydrophobicity. *J. Biomater. Sci. Polym. Ed.* **24**, 37–41 (2013).
13. Nagao, M. et al. Synthesis of highly biocompatible and temperature-responsive physical gels for cryopreservation and 3D cell culture. *ACS Appl. Bio Mater.* **1**, 356–366 (2018).
14. Zhao, J., Johnson, M. A., Fisher, R., Burke, N. A. D. & Stöver, H. D. H. Synthetic polyampholytes as macromolecular cryoprotective agents. *Langmuir* **35**, 1807–1817 (2019).
15. Vorontsov, D. A., Sazaki, G., Hyon, S.-H., Matsumura, K. & Furukawa, Y. Antifreeze effect of carboxylated epsilon-poly-L-lysine on the growth kinetics of ice crystals. *J. Phys. Chem. B* **118**, 10240–10249 (2014).
16. Stubbs, C., Bailey, T. L., Murray, K. & Gibson, M. I. Polyampholytes as emerging macromolecular cryoprotectants. *Biomacromolecules* **21**, 7–17 (2020).
17. Bailey, T. L. et al. A synthetically scalable poly(ampholyte) which dramatically enhances cellular cryopreservation. *Biomacromolecules* **20**, 3104–3114 (2019).
18. Matsumura, K. et al. Cryopreservation of a two-dimensional monolayer using a slow vitrification method with polyampholyte to inhibit ice crystal formation. *ACS Biomater. Sci. Eng.* **2**, 1023–1029 (2016).
19. Deller, R. C., Vatish, M., Mitchell, D. A. & Gibson, M. I. Synthetic polymers enable non-vitreous cellular cryopreservation by reducing ice crystal growth during thawing. *Nat. Commun.* **5**, 3244 (2014).
20. Mitchell, D. E., Lilliman, M., Spain, S. G. & Gibson, M. I. Quantitative study on the antifreeze protein mimetic ice growth inhibition properties of poly (ampholytes) derived from vinyl-based polymers. *Biomater. Sci.* **2**, 1787–1795 (2014).

21. Graham, B. et al. Polyproline as a minimal antifreeze protein mimic that enhances the cryopreservation of cell monolayers. *Angew. Chem. Int. Ed. Engl.* **56**, 15941–15944 (2017).
22. Ampaw, A., Charlton, T. A., Briard, J. G. & Ben, R. N. Designing the next generation of cryoprotectants—from proteins to small molecules. *Pept. Sci.* **111**, e24086 (2019).
23. Poisson, J. S., Briard, J. G., Turner, T. R., Acker, J. P. & Ben, R. N. Hydroxyethyl starch supplemented with ice recrystallization inhibitors greatly improves cryopreservation of human red blood cells. *Bioprocess. J.* **15**, 16–21 (2017).
24. Burkey, A. A. et al. Mechanism of polymer-mediated cryopreservation using poly(methyl glycidyl sulfoxide). *Biomacromolecules* **21**, 3047–3055 (2020).
25. Mazur, P. The role of intracellular freezing in the death of cells cooled at supraoptimal rates. *Cryobiology* **14**, 251–272 (1977).
26. Muldrew, K. & McGann, L. E. Mechanisms of intracellular ice formation. *Biophys. J.* **57**, 525–532 (1990).
27. Pegg, D. Cryopreservation. in *Essentials of Tissue Banking* (ed Galea, G.) 109–121 (Springer Netherlands, 2010).
28. Englezos, P. The freeze concentration process and its applications. *Dev. Chem. Eng. Miner. Process.* **2**, 3–15 (1994).
29. Ahmed, S., Hayashi, F., Nagashima, T. & Matsumura, K. Protein cytoplasmic delivery using polyampholyte nanoparticles and freeze concentration. *Biomaterials* **35**, 6508–6518 (2014).
30. Ahmed, S., Miyawaki, O. & Matsumura, K. Enhanced adsorption of a protein-nanocarrier complex onto cell membranes through a high freeze concentration by a polyampholyte cryoprotectant. *Langmuir* **34**, 2352–2362 (2018).
31. Stiff, P. J., Murgo, A. J., Zaroulis, C. G., DeRisi, M. F. & Clarkson, B. D. Unfractionated human marrow cell cryopreservation using dimethylsulfoxide and hydroxyethyl starch. *Cryobiology* **20**, 17–24 (1983).
32. Stolzing, A., Naaldijk, Y., Fedorova, V. & Sethe, S. Hydroxyethylstarch in cryopreservation—mechanisms, benefits and problems. *Transfus. Apher. Sci.* **46**, 137–147 (2012).
33. Boothby, T. C. et al. Tardigrades use intrinsically disordered proteins to survive desiccation. *Mol. Cell* **65**, 975–984 (2017). e5.
34. Yuen, F. et al. Preferential adsorption to air-water interfaces: a novel cryoprotective mechanism for LEA proteins. *Biochem. J.* **476**, 1121–1135 (2019).
35. Goyal, K., Walton, L. J. & Tunnacliffe, A. LEA proteins prevent protein aggregation due to water stress. *Biochem. J.* **388**, 151–157 (2005).
36. Tolleter, D., Hincha, D. K. & Macherel, D. A mitochondrial late embryogenesis abundant protein stabilizes model membranes in the dry state. *Biochim. Biophys. Acta* **1798**, 1926–1933 (2010).
37. Colletti, R. F. & Mathias, L. J. Solid-state 2H NMR: overview with specific examples. in *Solid State NMR of Polymers* (ed Mathias, L. J.) 23–60 (Springer US, 1991).
38. Hu, K.-N. & Tycko, R. What can solid state NMR contribute to our understanding of protein folding? *Biophys. Chem.* **151**, 10–21 (2010).
39. Mazur, P., Pinn, I. L. & Kleinhans, F. W. Intracellular ice formation in mouse oocytes subjected to interrupted rapid cooling. *Cryobiology* **55**, 158–166 (2007).
40. Stott, S. L. & Karlsson, J. O. M. Visualization of intracellular ice formation using high-speed video cryomicroscopy. *Cryobiology* **58**, 84–95 (2009).
41. Aksnes, D. W. & Gjerdåker, L. NMR line width, relaxation and diffusion studies of cyclohexane confined in porous silica. *J. Mol. Struct.* **475**, 27–34 (1999).
42. Miyatou, T. et al. study on the mechanisms of freezing and melting of water confined in spherically mesoporous silicas SBA-16. *Phys. Chem. Chem. Phys.* **18**, 18555–18562 (2016).
43. McMillan, J. A. & Los, S. C. Vitreous ice: irreversible transformations during warm-up. *Nature* **206**, 806–807 (1965).
44. Bloembergen, N., Purcell, E. M. & Pound, R. V. Relaxation effects in nuclear magnetic resonance absorption. *Phys. Rev.* **73**, 679–712 (1948).
45. Solomon, I. Relaxation processes in a system of two spins. *Phys. Rev.* **99**, 559–565 (1955).
46. Cocks, F. H. & Brower, W. E. Phase diagram relationships in cryobiology. *Cryobiology* **11**, 340–358 (1974).
47. Morales, D. J. & Greenbaum, S. NMR investigations of crystalline and glassy solid electrolytes for lithium batteries: a brief review. *Int. J. Mol. Sci.* **21**, 3402 (2020).
48. Naumann, C. & Kuchel, P. W. NMR of Na+, glycine and HDO in isotropic and anisotropic carrageenan gels. *Polym. Chem.* **1**, 1109–1116 (2010).
49. Patwari, G. N. & Lisy, J. M. Mimicking the solvation of aqueous Na+ in the gas phase. *J. Chem. Phys.* **118**, 8555–8558 (2003).
50. Driesner, T., Seward, T. M. & Tironi, I. G. Molecular dynamics simulation study of ionic hydration and ion association in dilute and 1 molal aqueous sodium chloride solutions from ambient to supercritical conditions. *Geochim. Cosmochim. Acta* **62**, 3095–3107 (1998).
51. Mandumpal, J. B., Kreck, C. A. & Mancera, R. L. A molecular mechanism of solvent cryoprotection in aqueous DMSO solutions. *Phys. Chem. Chem. Phys.* **13**, 3839–3842 (2011).
52. Wowk, B. Thermodynamic aspects of vitrification. *Cryobiology* **60**, 11–22 (2010).
53. Shinyashiki, N. et al. Glass transitions in aqueous solutions of protein (bovine serum albumin). *J. Phys. Chem. B* **113**, 14448–14456 (2009).
54. Toner, M., Cravalho, E. G. & Karel, M. Thermodynamics and kinetics of intracellular ice formation during freezing of biological cells. *J. Appl. Phys.* **67**, 1582–1593 (1990).
55. Jenekhe, S. A. & Roberts, M. F. Effects of intermolecular forces on the glass transition of polymers. *Macromolecules* **26**, 4981–4983 (1993).
56. Slark, A. T. The effect of intermolecular forces on the glass transition of solute-polymer blends: 2. Extension to different solutes. *Polymer* **38**, 4477–4483 (1997).
57. Chee, K. K. Dependence of glass transition temperature on chain flexibility and intermolecular interactions in polymers. *J. Appl. Polym. Sci.* **43**, 1205–1208 (1991).
58. Matsumura, K. et al. Molecular design of polyampholytes for vitrification-induced preservation of three-dimensional cell constructs without using liquid nitrogen. *Biomacromolecules* **21**, 3017–3025 (2020).
59. Hayashi, A. et al. Development of an efficient vitrification method for chondrocyte sheets for clinical application. *Regen. Ther.* **14**, 215–221 (2020).
60. Watanabe, H. et al. Efficient production of live offspring from mouse oocytes vitrified with a novel cryoprotective agent, carboxylated ε-poly-L-lysine. *PLoS ONE* **8**, e83613 (2013).
61. Tolleter, D. et al. Structure and function of a mitochondrial late embryogenesis abundant protein are revealed by desiccation. *Plant Cell* **19**, 1580–1589 (2007).
62. Furuki, T., Shimizu, T., Kikawada, T., Okuda, T. & Sakurai, M. Salt effects on the structural and thermodynamic properties of a group 3 LEA protein model peptide. *Biochemistry* **50**, 7093–7103 (2011).
63. Liu, Y., Chakrabortee, S., Li, R., Zheng, Y. & Tunnacliffe, A. Both plant and animal LEA proteins act as kinetic stabilisers of polyglutamine-dependent protein aggregation. *FEBS Lett.* **585**, 630–634 (2011).
64. Crowe, L. M., Reid, D. S. & Crowe, J. H. Is trehalose special for preserving dry biomaterials? *Biophys. J.* **71**, 2087–2093 (1996).
65. Drake, A. C. et al. Effect of water content on the glass transition temperature of mixtures of sugars, polymers, and penetrating cryoprotectants in physiological buffer. *PLoS ONE* **13**, e0190713 (2018).
66. Habeeb, A. F. S. A. Determination of free amino groups in proteins by trinitrobenzenesulfonic acid. *Anal. Biochem.* **14**, 328–336 (1966).
67. Delaglio, F. et al. NMRPipe: a multidimensional spectral processing system based on UNIX pipes. *J. Biomol. NMR* **6**, 277–293 (1995).
68. Johnson, B. A. Using NMR view to visualize and analyze the NMR spectra of macromolecules. in *Protein NMR Techniques* (ed Downing, A. K.) 313–352 (Humana Press, 2004).

Acknowledgements

This study was supported in part by a Grant-in-Aid, KAKENHI (Grant nos. 25870267 and 20H04532), for scientific research from the Japan Society for the Promotion of Science, a grant from the Canon Foundation (K11-N-028), and as a Collaborative Research Project organized by the Interuniversity Bio-Backup Project (IBBP). The NMR experiments were supported by grants and subsidies (Proposal No. 08-100-029, 11-500-019) for 'Open Advanced Research Facilities' from the Ministry of Education, Culture, Sports, Science and Technology, Japan.

Author contributions

K.M., F.H., and S.H.H. conceived the idea, K.M., F.H., and T.N. designed the experiments, K.M. prepared the materials and carried out cell analyses, F.H. and T.N. performed the NMR experiments, and K.M., F.H., and R.R. wrote the paper.

Competing interests

The authors declare no competing interests.

Additional information

Supplementary information The online version contains supplementary material available at https://doi.org/10.1038/s43246-021-00118-1.

Correspondence and requests for materials should be addressed to K.M.

Peer review information Primary handling editor: John Plummer

Reprints and permission information is available at http://www.nature.com/reprints

Publisher's note Springer Nature remains neutral with regard to jurisdictional claims in published maps and institutional affiliations.